Frequency and voltage regulation in hybrid AC/DC networks

Jeremy D. Watson and Ioannis Lestas

Abstract—Hybrid AC/DC networks are a key technology for sustainable electrical power systems, due to the increasing number of converter-based distributed energy resources such as solar or wind. In this paper, we consider the design of control schemes for hybrid AC/DC networks, focusing especially on the control of the interlinking converters (ILC(s)). We present two control schemes: firstly for decentralized primary control, and secondly, a distributed controller to achieve secondary control objectives as well. In the primary case, the stability of the controlled system is proven in a general hybrid AC/DC network which may include asynchronous AC subsystems. Furthermore, it is demonstrated that power-sharing across the AC/DC network is significantly improved compared to previously proposed dual droop control. The proposed scheme for secondary control guarantees the convergence of the AC system frequencies and the average DC voltage of each DC subsystem to their nominal values respectively. An optimal power allocation is also achieved at steady-state. The applicability and effectiveness of the proposed algorithms are verified by advanced simulations on a test hybrid AC/DC network in Simscape Power Systems.

Index Terms—AC/DC grids, frequency control, voltage control, distributed control

I. INTRODUCTION

Motivation: In view of the increasing number of converter-interfaced energy sources such as solar or wind generation, hybrid AC/DC networks are a key technology for sustainable electrical power systems. The hybrid AC/DC network allows the easy integration of such renewable energy sources and can combine the advantages of both DC grids and AC grids into one power network which operates with high efficiency. Direct current grids have several advantages [2] over traditional AC systems: lower power losses, largely due to the absence of reactive power; higher power transfer capability; and DC grids can also facilitate the connection of asynchronous AC grids. However, AC technology is well established and is more suitable for some applications. Therefore, it is advantageous to combine AC and DC networks via interlinking voltage source converters (VSC) to form a hybrid AC/DC network [3].

Hybrid AC/DC networks present new challenges in terms of frequency and voltage control [4]. In particular, an open problem [5] is the control of the interlinking converter (ILC), where the aim is to guarantee stability while ensuring that the

frequency and voltages are appropriately regulated. This is a challenging problem since the ILC operation simultaneously affects the AC frequency and the DC voltage. Moreover, a prescribed allocation is desired in many cases, such that economic optimality is achieved among generating units. Furthermore, distributed techniques for generation control are desirable due to the increasing penetration of renewable sources of generation which significantly increases the number of active elements in power grids, making traditional centralized approaches impractical and costly.

Related work: Numerous controllers for either AC or DC networks or microgrids alone have been proposed recently, e.g. from simple droop-based strategies to sliding mode control for DC networks in [6], distributed consensus for DC networks in [7]-[8], and model predictive control in [9]. For AC microgrids the literature is even more extensive, as surveyed in [10] for example. However, we focus on the control of hybrid AC/DC network, which presents new challenges as control actions on either the AC or DC sides affect the entire network. It is also more difficult to achieve optimality of power allocation between AC and DC sources.

Both primary and secondary control strategies are required for AC/DC networks. In comparison to the literature on AC networks or DC networks, relatively few control approaches for AC/DC networks have been proposed, especially for secondary control. Such control schemes are implemented via the AC / DC sources in conjunction with the ILC and must regulate the AC frequency, DC voltage, and power allocations. We briefly review the primary and secondary control schemes in the literature for the ILC.

Droop control schemes are decentralized, intuitive, and easy to implement. AC frequency droop is ubiquitous, while DC voltage droop controllers are prevalent in the literature as well. The DC bus voltage dynamics are comparable to traditional AC frequency / real power control, in that an excess of active power increases the voltage and vice versa. Hence, an obvious way to control the interlinking converter is a dual droop scheme combining the two characteristics in one controller. The DC voltage droop stabilizes the DC grid and the DC system participates in the frequency regulation of the connected AC grids via the ILC [11]. However, the two droop schemes interact with each other in a way that degrades their performance, as noticed by [12]. A strategy using the ILC power to improve performance is presented in [13], although the coupling between the AC and DC grids still introduces some inaccuracy.

Another approach for the control of the ILCs was presented in [3], [16], and [17], where the per-unit values of the AC

frequency and DC voltage are synchronized by controlling the power transfers through the ILC with a proportional-integral (PI) controller. This allows the ILC to relate the AC frequencies and DC voltages to each other; and the power allocation is then determined by the droop coefficients of the AC and DC sources. This approach is effective, although the slower integral term makes the use of inertia through the ILC difficult to achieve.

A similar strategy has also been proposed for secondary control, where the aim is to restore the frequencies and voltages to their nominal value and to share power equitably between sources in the AC and DC subsystems [4]. A distributed consensus approach was proposed in [14], where again the AC frequency and DC voltage are synchronized by PI control of the ILC. This approach is effective for a AC / DC networks with only one ILC bus connection. However, in the case of DC subsystems with multiple interconnections at different buses, regulating the local voltage deviations to zero via the ILC is not optimal because this affects the power transfer capability through such a DC subsystem. In [18], a distributed controller for sharing frequency reserves of asynchronous AC systems via HVDC was designed. However the DC voltage dynamics were not modelled. The authors in [19] designed distributed controllers for distributed frequency control of asynchronous AC systems connected through a MTDC grid.

Contribution: In view of the current literature, there is a need for new control schemes which: can be rigorously proven to be stable in any AC/DC network topology; can achieve an appropriate steady-state power allocation without the use of communication; and can make use of the DC system(s) and ILC(s) to provide inertia for the AC system(s) and vice versa [20].

In this paper, we present new voltage source converter control schemes for the interlinking converters in hybrid AC/DC networks. Inspired by the controller proposed in [21], where linking the DC voltage to the AC frequency was found to provide desirable stability and performance properties in AC networks, we show the successful application of similar ideas to general hybrid AC/DC networks for both primary and secondary control. The proposed schemes have advantages over previous proposals, including the existence of rigorous stability guarantees in general network topologies, improved power sharing, and the ability of the proposed controllers to use the energy stored in the DC capacitance as the "inertia" for the emulation of synchronous machines. In particular, our decentralized control approach, by making use of the energy stored in DC-side capacitance, achieves an improved steady-state power allocation and primary frequency regulation compared to schemes that directly control the power transfer. We also propose a scheme for distributed secondary frequency and voltage control which regulates the frequency and the weighted average voltages of DC subgrids to prescribed nominal values at steady state, and also leads to an optimal power sharing. Moreover, we show that virtual capacitance in the controller can be used to further improve performance.

For clarity, we summarize the main contributions of the paper below:

1) We propose a decentralized VSC controller inspired by [21] for general hybrid AC/DC networks. For this setting, we provide stability guarantees and sufficient conditions for an optimal steady state power allocation.

2) We propose a novel distributed approach for the control of interlinking converters and generation sources for secondary frequency and voltage regulation which guarantees the convergence of both the AC system frequencies and the weighted average DC voltage of each DC subsystem to their nominal values. A prescribed power sharing is also achieved. We also show that virtual capacitance in the controller can be used to adjust the voltage deviations and improve performance.

3) We perform realistic simulations with advanced converter and generator models in a suitable test system, verifying the performance of our control strategies and comparing them to the traditional dual-droop controller.

Paper structure: The paper is organized as follows. Section II presents the network model and formulates the control problem. Our main results are given in section III, including the proposed decentralized primary controller in section III-A and the distributed controller in section III-B. The performance of the two controllers is illustrated via case studies in section IV and compared to traditional controllers. Finally, conclusions are presented in section V. The proofs of all the results presented can be found in the appendix.

II. PROBLEM FORMULATION

A. Network model

We consider a general hybrid AC/DC network with the set of buses denoted by $N = (1, 2, ..., |N|)$ and the set of transmission lines by $E = (1, 2, ..., |E|)$. The network is composed of multiple AC and DC subsystems. We denote the set of subsystems by $K = (1, 2, ..., |K|)$ and we also have $N = (\cup_i N_i^{dc}) \cup (\cup_j N_j^{ac})$, where N_i^{ac} and N_j^{dc} denote the collection of buses belonging to the AC subsystem $i \in K$ and DC subsystem $j \in K$ respectively. Each subsystem is assumed to be connected and it is connected to the rest of the network only via interlinking converters[1], as illustrated in Figure 1. Each AC subsystem i is described by the connected graph (N_i^{ac}, E_i^{ac}) with arbitrary direction, and each DC subsystem j by the connected graph (N_j^{dc}, E_j^{dc}) with arbitrary direction[2]. For each bus $j \in N$ we use $i : i \to j$ and $k : j \to k$ to denote the predecessors and successors of bus j respectively. For convenience we also define the set of all AC buses $N_{ac} = \cup_i N_i^{ac}$ and all DC buses $N_{dc} = \cup_j N_j^{dc}$, such that $N_{ac} \cup N_{dc} = N$; likewise we define the set of all AC edges $E_{ac} = \cup_i E_i^{ac}$ and all DC edges $E_{dc} = \cup_j E_j^{dc}$. Connections between AC and DC buses are facilitated by the interlinking converters, the set of which is denoted by $X = (1, 2, ..., |X|)$. The ILC buses are denoted by $X_j^{ac} \in N_{ac}$ and $X_j^{dc} \in N_{dc}$ for the AC and DC buses, respectively, to which the ILC j is connected. The set of AC buses to which a converter is connected is denoted by $X_{ac} = (X_1^{ac}, ..., X_{|X|}^{ac}) \subset N_{ac}$. Similarly, the set

---

[1]Note that this is without loss of generality since the connection of two collections of AC buses (or DC buses respectively) may simply be considered as one larger subsystem.

[2]The results presented in the paper are unaffected by the choice of direction.

of DC buses to which a converter is connected is denoted by $X_{dc} = (X_1^{dc}, \ldots, X_{|X|}^{dc}) \subset N_{dc}$.

Table I
NOTATION IN SYSTEM MODEL

ω_j	AC frequency deviation at bus j
η_{ij}	voltage angle between two AC buses i and j
M_j	inertia at bus j
p_j^G	generated power at bus j
p_j^L	load power at bus j
p_j^X	interlinking converter power transfer at bus j
p_{ij}	power transfer between buses i and j
B_{ij}	transmission line susceptance for $(i,j) \in E_{ac}$
D_j	damping coefficient at bus $j \in N_{ac} \setminus X_{ac}$
C_j	capacitance at bus $j \in N_{dc}$
V_j	DC voltage deviation at bus j
G_{ij}	line conductance for $(i,j) \in E_{dc}$

Assumption 1. *We make the following assumptions regarding the network:*

- *1a: Voltage magnitudes are 1 p.u. for all buses $j \in N_{ac}$.*
- *1b: Lines $(i,j) \in E_{ac}$ are lossless and are characterized by their constant reactances $X_{ij} > 0$.*
- *1c: Reactive power does not affect either bus voltage angles or the frequency, and is thus ignored.*
- *1d: The AC system(s) are three-phase balanced.*
- *1e: Bus voltages are close to 1 p.u. for all $j \in N_{dc}$, such that currents and powers are approximately equivalent in a per-unit system.*
- *1f: Lines $(i,j) \in E_{dc}$ are characterized by their conductance $G_{ij} = \frac{1}{R_{ij}}$, where R_{ij} is the line resistance. The line losses are small and may be neglected.*

Remark 1: Assumption 1 may be explained as follows:

- 1a-d: These are well-known assumptions for AC transmission systems which are used in much of the literature. These assumptions allow us to model the active power transfer through a line (i,j) as $p_{ij} = B_{ij} \sin \eta_{ij}$ where $B_{ij} = 3X_{ij}^{-1} > 0$.
- 1e-f: These are typical assumptions in DC networks [19], making use of the fact that in practice the DC grid voltage will typically be regulated very close to the nominal and that line losses are generally small. In particular, although the percentage change in DC voltage differences between buses can be large (and thus cannot be ignored), the percentage change in individual DC voltages is small (also demonstrated in our simulations in Section IV with the proposed controller). [3]

We also consider the modelling of the interlinking converters, as illustrated in Fig. 1. The AC-side bus of the interlinking converter has no inertia of its own, however power imbalances in the AC subsystem lead to a power transfer through the converter. Note also that this power transfer will affect the DC-side voltage of the converter. For each bus $j \in X_{ac} \cup X_{dc}$, we define the power transfer p_j^X as the power leaving the bus

---

[3]In networks where 1e is not applicable, the DC network flows may be represented by currents instead of power. The proof of stability in Theorem 1 would then require a passivity condition from the input voltage to output current at each DC bus, along with a similar condition on the ILC equations.

---

through the ILC. Hence for a converter bus $j \in X_{ac}$, the power transfer p_j^X is the AC-to-DC transfer, whereas for a converter bus $j \in X_{dc}$, the power transfer p_j^X is the DC-to-AC transfer. We assume that such power transfers are instantaneous and lossless, hence for an ILC x we have $p_{X_x^{dc}}^X = -p_{X_x^{ac}}^X$.
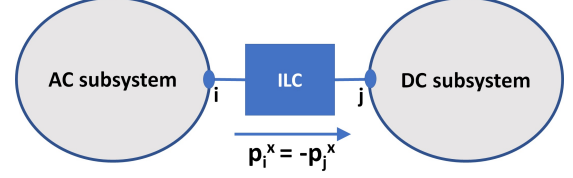

Figure 1. ILC connection diagram

Given these assumptions and definitions, the hybrid AC/DC network dynamics are:

$$\dot{\eta}_{ij} = \omega_i - \omega_j, (i,j) \in E_{ac} \tag{1a}$$

$$M_j \dot{\omega}_j = p_j^G - p_j^L + \sum_{i:i \to j} p_{ij} - \sum_{k:j \to k} p_{jk} - D_j \omega_j,$$
$$j \in N_{ac} \setminus X_{ac} \tag{1b}$$

$$0 = p_j^G - p_j^L + \sum_{i:i \to j} p_{ij} - \sum_{k:j \to k} p_{jk} - p_j^X, j \in X_{ac} \tag{1c}$$

$$C_j \dot{V}_j = p_j^G - p_j^L + \sum_{i:i \to j} p_{ij} - \sum_{k:j \to k} p_{jk} - p_j^X, j \in N_{dc} \tag{1d}$$

$$p_{ij} = \begin{cases} B_{ij} \sin \eta_{ij} & j \in N_{ac} \\ G_{ij}(V_i - V_j) & j \in N_{dc} \end{cases}, (i,j) \in E \tag{1e}$$

We now write the system dynamics in matrix form. The vector of angle differences is $\eta = [\eta_{ij}]_{(i,j) \in E_{ac}}$, the vector of AC frequency deviations from its nominal value (50 or 60 Hz) is denoted by $\omega = [\omega_j]_{j \in N_{ac}}$, while the vector of DC voltage deviations from their nominal value is denoted by $V = [V_j]_{j \in N_{dc}}$. M is the diagonal matrix of the generator inertias $M_j, j \in N_{ac} \setminus X_{ac}$, while the damping coefficients are $D = diag([D_j]_{j \in N_{ac} \setminus X_{ac}})$. The frequencies at the corresponding AC buses are denoted by $\omega^G = [\omega_j]_{j \in N_{ac} \setminus X_{ac}}$, and the vector of frequencies at the converter buses is $\omega^X = [\omega_j]_{j \in X_{ac}}$. The diagonal matrix of the DC bus capacitances is $C = diag([C_j]_{j \in N_{dc}})$. The vector of generator powers is denoted by $p^G = [p_j^G]_{j \in N}$, the vector of load powers by $p^L = [p_j^L]_{j \in N}$. We also use the notation $p_j^X = 0$ for buses without converters, i.e. $j \in N \setminus (X_{ac} \cup X_{dc})$ and denote the vector of converter powers by $p^X = [p_j^X]_{j \in N}$. Similarly, at the converter buses $j \in X_{ac}$ we use the notation $p_j^G = 0$. The power transfer vector is defined by $p^F = [p_j^F]_{j \in N}$, where each $p_j^F = \sum_{i:i \to j} p_{ij} - \sum_{k:j \to k} p_{jk}$. The matrix A is the incidence matrix of the graph (N_{ac}, E_{ac}). The system equations are thus:

$$\dot{\eta} = A^T \omega = A^T \begin{bmatrix} \omega^G \\ \omega^X \end{bmatrix} \tag{2a}$$

$$\begin{bmatrix} M\dot{\omega}^G \\ 0 \\ C\dot{V} \end{bmatrix} = p^G - p^L - p^X + p^F - \begin{bmatrix} D\omega^G \\ 0 \\ 0 \end{bmatrix} \tag{2b}$$

1) Equilibrium conditions: An equilibrium of the system in (2) is defined by the following conditions:

$$0 = A^T \omega = A^T \begin{bmatrix} \omega^G \\ \omega^X \end{bmatrix} \tag{3a}$$

$$0 = p^G - p^L - p^X + p^F - \begin{bmatrix} D\omega^G \\ 0 \\ 0 \end{bmatrix} \tag{3b}$$

We assume that there exists[4] some equilibrium point of (2), and denote such an equilibrium by $(\eta^*, \omega^{G*}, V^*)$. Individual equilibrium values are also denoted by the superscript asterisk, e.g. η_{ij}^*, ω_i^{G*}, and V_j^*.

Assumption 2. $|\eta_{ij}^*| < \frac{\pi}{2}$ *for all* $(i, j) \in E_{ac}$.

This assumption is often referred as a security constraint and is common in the literature for power grid stability analysis.

B. Control objectives

The control objectives are:

1) Solutions must converge to an equilibrium point.
2) For primary control, AC frequencies and DC voltages should not deviate too far from their nominal values, i.e. $\lim_{t\to\infty} |\omega_j(t)| < e_\omega$ for all buses $j \in N_{ac}$ and $\lim_{t\to\infty} |V_j(t)| < e_V$ for all buses $j \in N_{dc}$ for some appropriate scalars e_V and e_ω.
3) AC frequencies and a weighted average of the DC voltages should converge to their nominal values for secondary control.
4) Power sharing between all sources should be optimal.

The last objective may be stated more formally by considering the minimization of a quadratic cost function [22]:

$$\min_{p^G} C_G = \frac{1}{2}(p^G)^T Q p^G \tag{4a}$$

$$\text{subject to: } \mathbf{1}^T p^G = \mathbf{1}^T p^L + \mathbf{1}^T \begin{bmatrix} D\omega^G \\ 0 \\ 0 \end{bmatrix} \tag{4b}$$

$$p_j^G = 0, j \in X_{ac} \tag{4c}$$

where Q is a positive definite diagonal matrix containing the cost coefficients for each energy resource, and $\mathbf{1}$ is the vector of ones with appropriate dimension, and $\mathbf{0}$ is the vector of zeros with appropriate dimension. Note that constraint (4b) is a requirement for power balance at equilibrium, i.e. that the total generation and demand are equal, while (4c) suggests that the generation at converter AC buses is zero, which holds by definition (note that p_j^G appears in (1c) only for convenience in presentation). To proceed further, we define the diagonal matrix $\tilde{Q}$ such that $\tilde{Q}_{ii} = Q_{ii}^{-1}, i \in N/X_{ac}$ and $\tilde{Q}_{ii} = 0, i \in X_{ac}$. With slight abuse of terminology, we shall refer to $\tilde{Q}$ as the inverse cost matrix.

[4]Existence of equilibria in AC systems is beyond the scope of this paper and have been considered in e.g. [23].

Using the standard method of Lagrange multipliers as in [22], and defining the vector $p^u = [(D\omega^G)^T \ \mathbf{0}^T \ \mathbf{0}^T]^T$ for convenience, the solution p^{G*} to the optimization problem is:

$$p^{G*} = \frac{\tilde{Q}\mathbf{1}\mathbf{1}^T}{\mathbf{1}^T \tilde{Q}\mathbf{1}}(p^L + p^u) \tag{5}$$

III. MAIN RESULTS

A. Decentralized primary control

We assume power-frequency droop control for the AC generators and power-voltage droop for the DC energy resources:

$$p^G = -\tilde{Q}\begin{bmatrix} \omega \\ mV \end{bmatrix} + p_{nom}^G \tag{6}$$

where $\tilde{Q} \geq 0$ is the inverse cost matrix of droop coefficients, and $m > 0$ is a constant, and as stated previously, ω and V are the column vectors of the AC frequency and DC voltage deviations, respectively. The nominal power generation p_{nom}^G is a constant reference of the droop control scheme that satisfies (4) for a nominal aggregate load[5] and with the frequencies at their nominal value.. The second control objective (limitation of frequencies and voltages deviations) may be satisfied by choosing suitably large droop coefficients in $\tilde{Q}$. In order to simplify the presentation here we use proportional droop control schemes, nevertheless this condition could be relaxed to local input strict passivity of the dynamics of each AC generator from input $-\omega_j$ to output p_j^G and each DC generator from input $-V_j$ to output p_j^G around their respective equilibrium values ω_j^* and V_j^*, similarly to the analysis in [24]. It should be noted that the majority of DC networks are voltage-controlled, i.e. each DC source regulates its output voltage (which may be droop based on current or voltage). Such voltage-controlled DC droop sources, along with more detailed dynamic models, can also be incorporated in our analysis if a strict passivity condition from the negative output power $-p_j^G$ (or current) to the bus voltage V_j is satisfied. This allows a wide range of DC droop control structures to be integrated [26].

We also introduce a VSC controller based on [21]. Let the voltage angle θ_i at the AC-side output of an ILC x be:

$$\theta_i = \int mV_j, \text{ i.e. the frequency is given by,} \tag{7a}$$

$$\omega_i = \dot{\theta}_i = mV_j \tag{7b}$$

where $i \in X_x^{ac}$ and $j \in X_x^{dc}$. This relates the AC frequency deviation proportionally to the DC voltage deviation by a chosen constant $m > 0$. Hence, (7b) necessitates that the frequency at the AC side of the ILC is set directly by the ILC, rather than controlling the power transfer through the ILC as in traditional ILC control schemes. The relationship between AC frequency and DC voltage allows to provide appropriate stability and optimality properties for the network, as we will show within the paper.

[5]Note that p_L in (1) does not need to be equal to the nominal load for power balance to be achieved at equilibrium, i.e. power balance will hold if an equilibrium point of (1),(6),(7) is reached with the power generated determined by the deviations in frequency/voltage.

We assume that the converter is lossless and that the internal dynamics are sufficiently fast compared to the network dynamics. In [21] the suggestion is to set $m = \frac{\omega^{nom}}{V_{dc}^{nom}}$ where ω^{nom} and V_{dc}^{nom} are the nominal values of the AC grid frequency and the DC grid voltage. Since in this paper ω_i and V_j are deviations from a nominal value, other values of m are also possible. Large values of m result in smaller DC voltage deviations and larger AC frequency deviations, and in general $m = \frac{\omega^{nom}}{V_{dc}^{nom}}$ may be too large for this scheme as frequency deviations are generally less acceptable than voltage deviations. Instead of directly controlling the power transfer, (7b) relates the frequency and voltage within the AC and DC sides, respectively. Not only does this improve the accuracy of the power-sharing in the primary time-frame, but also provides fast response to AC disturbances via capacitive inertia as discussed in [21] and [22]. In this paper, we take this concept further and use the capacitive inertia of the entire DC subsystem for frequency support, and also use the inertia of the AC system to regulate the DC voltage when appropriate.

Theorem 1 (Stability). *Consider a dynamical system described by equations* (1), (2) *with the control scheme in (6), (7b), and an equilibrium point for which Assumption 2 holds. Then there exists an open neighbourhood of this equilibrium point such that all solutions of* (1),(2),(6),(7b) *starting in this region converge to the set of equilibrium points as defined in* (3).

Theorem 1 demonstrates the local convergence of solutions to (1),(2),(6),(7b) to the set of its equilibria. Note that the result is local due to the sinusoidal power transfers in (1e) and that it becomes global if those are linearized.

The following theorem demonstrates that when line resistances become arbitrarily small, then the equilibria of the considered system tend towards the global minimum of (4).

Theorem 2 (Power sharing). *As the DC line resistances become arbitrarily small, the power sharing of the system* (1), (2) *with the control scheme (6), (7b) becomes arbitrarily close to the solution of the optimization problem* (4).

Remark 2: In a practical network there will always be some small DC line resistances which affect power sharing. A fundamental trade-off exists between voltage regulation and power sharing accuracy for linear droop-controlled DC grids [27]-[28] which can be adjusted by changing the magnitude of droop gains. Nevertheless, if these line resistances are small, the voltage deviations will also be small and the power sharing will be close to optimal.

Remark 3 (Power sharing in a dual-droop ILC controller scheme): Consider the dual-droop scheme (8) often used in the literature for primary control of the ILC,

$$p_i^X = K_i^\omega \omega_i - K_j^V V_j \tag{8}$$

where K_i^ω and K_j^V are the respective droop coefficients, and the power transfer is directly controlled[6]. It is clear that (8) is unable to guarantee correct power-sharing for a disturbance

[6]In practice, the ILC controls the power transfer by varying its output voltage angle until (8) is satisfied.

at any arbitrary bus under the same assumptions. For droop-controlled sources to contribute power in proportion to their droop coefficients, a system-wide synchronizing variable is required. The proposed controller (7b) achieves this by relating the AC frequency to the DC voltages. By contrast, the dual droop controller (8) does not provide such a relation.

B. Distributed control

In this section we propose a distributed controller inspired by [22] and [25]. The controller proposed in this section uses communication to achieve the secondary control objectives of exact power sharing, frequency and voltage regulation. It should be noted that this scheme is an alternative to that of the communication-free scheme in section III-A and should therefore be used if appropriate communication is available.

The concept of *network emulation* can be carried further with the aid of distributed communication. Let the average DC voltage deviation of each subsystem k be represented by the capacitance-weighted average $\bar{V}_k$:

$$\bar{V}_k = \sum_{j \in N_k^{dc}} C_j V_j \tag{9}$$

As in the second distributed MTDC controller proposed in [25], the DC voltages within each subsystem are either communicated within the network so as to obtain $\bar{V}_k$ (for small subsystems) or $\bar{V}_k$ is obtained via an appropriately fast distributed approach, such that its dynamics can be decoupled from the stability analysis in this paper. From (9) we have:

$$\dot{\bar{V}}_k = \sum_{j \in N_k^{dc}} C_j \dot{V}_j = \sum_{j \in N_k^{dc}} (p_j^G - p_j^L - p_j^X + p_j^F) \tag{10}$$

The DC branch-flows p_j^F cancel out within the subsystem, and we therefore have the following expression which resembles the swing equation:

$$\dot{\bar{V}}_k = \sum_{j \in N_k^{dc}} (p_j^G - p_j^L - p_j^X) \tag{11}$$

We now introduce the concept of *virtual frequency deviation* $\hat{\omega}$ which is defined for the entire network as follows:

$$\hat{\omega}_j = \begin{cases} \omega_j & \text{if } j \in N_{ac} \\ m\bar{V}_k & \text{if } j \in N_k^{dc} \end{cases} \tag{12}$$

where k is the DC subsystem to which all nodes in the associated set N_k^{dc} belong. We will denote the vector of average DC subsystem voltages by $\bar{V}$. The converter which interlinks AC bus i and the DC subsystem k is governed by

$$\omega_i = m\bar{V}_k \tag{13}$$

where $m > 0$ is a positive coefficient. Similarly to the primary controller (7), we control the AC frequency of the interlinking converter instead of directly controlling the power transfer. A common approach to achieve optimal power sharing in secondary control is to introduce a synchronizing communicating variable ξ, e.g. [22], and update these values via distributed averaging through an undirected connected communication graph. In particular, we denote this graph by $(N, \tilde{E})$, where

$\tilde{E}$ denotes the set of communication links, and also denote by $\mathcal{L}$ the Laplacian of $(N, \tilde{E})$, defined as

$$\mathcal{L}_{ij} = \begin{cases} \deg(i), & \text{if } i = j, \\ -1, & \text{if } (i, j) \in \tilde{E} \\ 0, & \text{otherwise} \end{cases} \quad (14)$$

where $\deg(i)$ denotes the degree of node i. Then the distributed controllers for the hybrid AC/DC system are:

$$T_\xi \dot{\xi} = -\mathcal{L}\xi - \tilde{Q}\hat{\omega} \quad (15a)$$
$$p^G = \tilde{Q}\xi - \mathcal{K}\hat{\omega} \quad (15b)$$

where T_ξ denotes the diagonal matrix with positive time constants, ξ is the column vector of the synchronizing variables ξ_j, and $\tilde{Q}$ is the inverse cost coefficient matrix as before and $\mathcal{K}$ is a diagonal matrix of positive coefficients used to improve performance and determine power contributions from each generator in the primary time-frame. The proportional term $\mathcal{K}\hat{\omega}$ is effectively a primary (droop) controller while the slower secondary term $\tilde{Q}\xi$ integrates the frequency and average voltage deviations to a steady-state value of zero, and leads also to an optimal power sharing (Theorem 3 below).

One interesting feature of this controller is that the DC bus voltages are weighted by the associated capacitances. This is in order to capture the dynamics of the physical energy of the subsystem as follows from (10). A potential objection could be that buses with low capacitance could have voltages far from the nominal while still satisfying $\bar{V}_k = 0$, due to their faster response. Nevertheless, small voltage deviations at such buses may still be maintained in two ways. Firstly, the steady-state DC bus voltages must still satisfy the power-flow equations. This is a constraint that does not depend on capacitances and can potentially restrict large voltage deviations (will be dependent on the power flows and line resistances). Secondly, virtual capacitance C_j^V may easily be added at any DC source bus j via a derivative term in the DC source dynamics, e.g.:

$$p_j^G = \tilde{Q}_{jj}\xi_j - \mathcal{K}_{jj}\hat{\omega}_j - C_j^V \dot{V}_j$$

The addition of the derivative term will not affect the steady-state value of p_j^G, allowing its optimality properties to be retained.

Our first result, proven in the appendix, demonstrates that the introduction of the controller (12),(13),(15) ensures that the equilibria of the system (2),(12),(13),(15) coincide with the global minimum of the optimization problem (4).

Theorem 3 (Power sharing). *An equilibrium of the system* (1),(2) *with the control scheme* (12),(13),(15) *solves the optimization problem* (4).

The following theorem, proven in the appendix, demonstrates the local convergence of solutions of the dynamical system (1),(2), when the controller (12),(13),(15) is applied, to the global minimum of the optimization problem (4). Furthermore, it guarantees that frequency returns to its nominal value at equilibrium, i.e. that $\omega^* = 0$, and that the average voltage deviation in every DC subsystem is zero, i.e. that $\bar{V}^* = 0$.

Theorem 4 (Convergence to optimality). *Consider the dynamical system described in* (1),(2) *with the control scheme* (12),(13),(15) *and an equilibrium point for which Assumption 2 is satisfied. Then, there exists an open neighbourhood of this equilibrium point such that all solutions of* (1),(2),(12),(13),(15) *starting in this region converge to a set of equilibria that solve the optimization problem* (4), *with* $\omega^* = 0$ *and* $\bar{V}^* = 0$.

Theorem 4 demonstrates that all solutions of the considered system locally converge to an optimal solution of (4).

Remark 4: Our proposed controller is distributed in the sense that its implementation in a DC subgrid makes use of voltage measurements only within that subgrid, and is also fully distributed in the AC subgrids of the network. It should be noted that relaxing (9) to a fully distributed controller that makes use of only local voltage measurements without additional information transfer, while retaining the stability and optimality properties presented, is a highly non-trivial problem as this would distort the synchronization of the communicating variable ξ needed for optimal power sharing.

IV. CASE STUDIES

In order to demonstrate our results, we study the performance of our controllers in two hybrid AC/DC systems, the first as shown in Fig. 2, and the second being the ring network in Fig. 3. All studies are carried out in MATLAB / Simscape Power Systems.
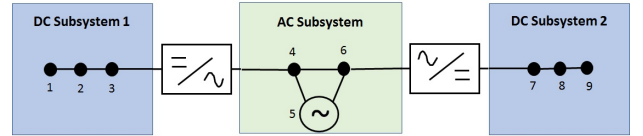

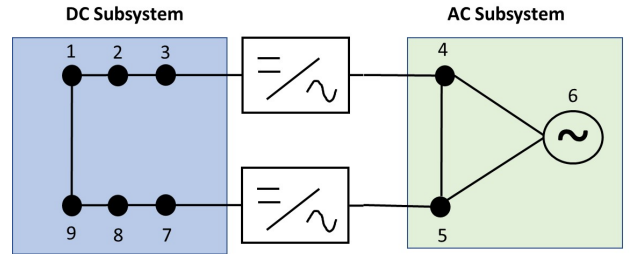Figure 2. Example AC/DC network 1 (mixed topology).

Figure 3. Example AC/DC network 2 (ring topology).

The parameters of the networks are given in Table II. For simplicity, we have chosen the same parameters for both networks and have numbered the buses such that the parameters and description of loads and generation applies to both networks. Varying line parameters within reasonable bounds does not significantly affect the performance of the controllers, except the effect on power sharing within the DC subsystem(s) in the primary time-frame, as expected [28]. The synchronous machine is 4 MVA, 13.8kV and is connected to the AC subsystem at bus 5 via a 4 MVA step-down transformer, and there are four distributed DC generators across the two subsystems at buses 1 and 9 (1 MW) and buses 3 and 7 (3 MW).

The simulation model is more detailed and realistic than our analytical model, and it includes the inverter dynamics with switching (two-level pulse width modulation), line dynamics, detailed generator, turbine-governor, and exciter dynamics, and realistic communication delays. The switching of the two-level PWM converters causes the DC ripple seen in some of the figures. More detailed parameters of the test system are given in Table IV.

Table II
HYBRID AC/DC NETWORK PARAMETERS

Description	Parameter	Value
Bus capacitances	C_1, C_3, C_7, C_9	6 mF
DC load resistances	$R_j, j \in N_{dc}$	600 Ω
DC line resistances	$R_{12}, R_{19}, R_{23}, R_{78}, R_{89}$	0.1 Ω
DC line inductances	$L_{12}, L_{19}, L_{23}, L_{78}, L_{89}$	1 mH
DC switched loads	P_3, P_7	1.2 MW
Rated DC voltage	V_{dc}^*	10 kV
Converter DC capacitances	C_3, C_7	2 mF
Converter AC filter parameters	$R(\Omega), L(mH), C(\mu F)$	0.1, 1, 10
Converter ω /V ratio	m	0.002
AC voltage	V_{ac}	3.3 kV
AC line resistances	R_{ij}	0.1 Ω
AC line inductances	L_{ij}	1 mH
AC load resistances (per phase)	R_4, R_6	1000 Ω
AC load active power	R_5	1 MW
Transformer reactance	X_5	4%
Generator inertia constant	M	3.2 s^{-1}
AC frequency	$f = \frac{\omega}{2\pi}$	50 Hz

A. Decentralized primary control

Using the controllers (6), (7b) we show that the voltages and frequencies converge to equilibrium values and that the power-sharing is close to the optimal values irrespective of the location of the disturbance. The droop coefficients in $\tilde{Q}$ are set proportionally to the source ratings with gains of (500 kW / (rad/s), 1 kW / V, 3 kW / V) for the synchronous generator, DC sources at buses 1 and 9, DC sources at buses 3 and 7 respectively. In Fig. 4 we show the AC frequency and DC voltage response to the same step disturbances at time $t = 3s$ and $t = 23s$. The magnitude of the disturbance at $t = 3s$ is 1.2 MW (nominal added demand) located at bus 3 within DC subsystem 1, while the disturbance $t = 23s$ is 1.2 MW reduced demand at bus 7 within DC subsystem 2. Fig. 5 shows that the power allocation converges to values close to proportional as required.
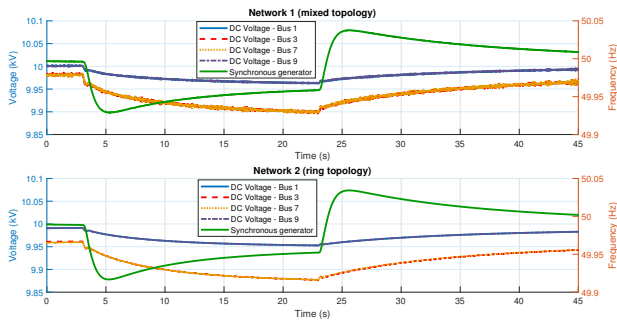

Figure 4. Frequency and voltage response with the decentralized primary controller (6),(7)

For comparison we also study the same hybrid AC/DC networks with traditional dual-droop controlled ILCs. The droop gains for the sources (250 kW / (rad/s), 500 W / V,
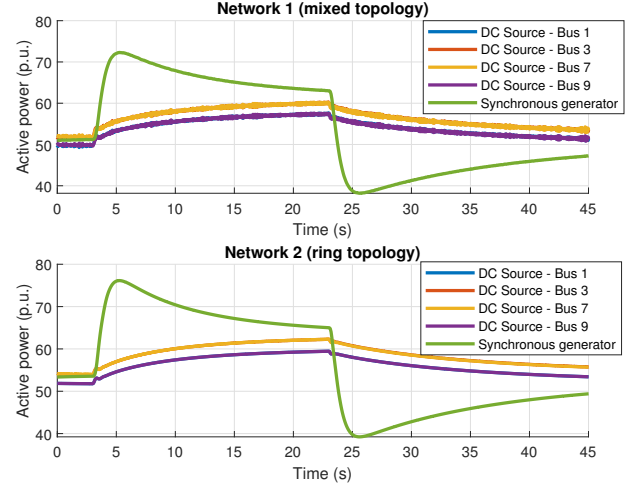

Figure 5. Power-sharing response with the decentralized primary controller (6),(7)

1500 W / V) and the dual-droop scheme (50 W / V, 250 kW / (rad/s)) are chosen to achieve a reasonable power-sharing (hence the smaller source droop gains and the large dual-droop gains). Note it is impossible to achieve comparable steady-state power-sharing to our proposed scheme. The other control parameters are then tuned to achieve the best possible performance. It is possible to improve either the transient performance or the power-sharing optimality, however both cannot be improved simultaneously. Figs. 6-7 show that the voltage / frequency deviations at equilibrium as well as the power sharing are inferior to the proposed method, with larger deviations and sub-optimal power-sharing. Increasing the droop gains decreases the voltage and frequency deviations at steady-state, however unacceptable oscillations were noted in simulations. Unlike with the proposed primary controller, the topology has a strong effect on the power sharing performance. The dual-droop control performs considerably worse in the first test network with three subsystems compared to the two subsystem ring network. In general, power sharing performance with dual-droop control is poorer in larger and more spread out networks with more subsystems, since no prescribed relation between the AC frequency and DC voltages is maintained among subsystems.
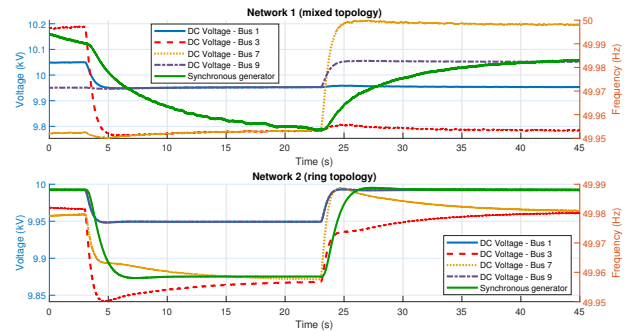

Figure 6. Frequency and voltage response with traditional dual-droop control (8)

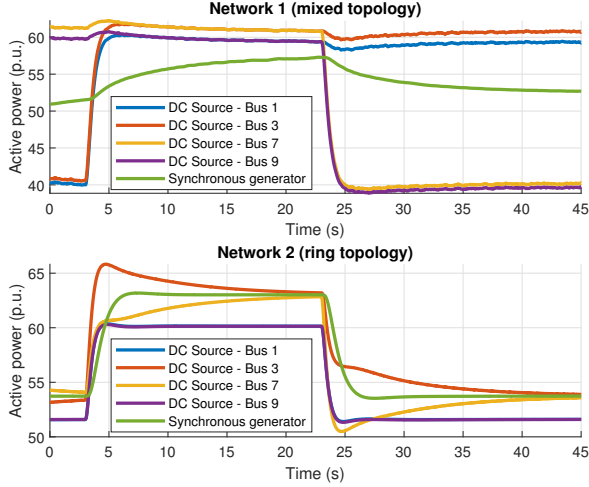The simulations show several advantages of our proposed

Figure 7. Power-sharing response with traditional dual-droop control (8)

Figure 8. Frequency and voltage response with the distributed secondary controller (13),(15)

primary controller. Firstly, the power requirement of any load change or disturbance can be effectively shared by sources across the entire hybrid AC/DC network. In contrast, the dual-droop scheme requires nearby sources to support most of the power requirement, which is not only less optimal but may also cause device ratings to be exceeded. Secondly, our proposed scheme is able to use the inertia of the synchronous machine and the capacitance of both DC subgrids to quickly contribute to the power balancing. As seen in Fig. 5, the inertia of the synchronous machine is used to supply the load demand in the first few seconds. Since synchronous machines are able to handle short-term overloads much more successfully than power-electronic converters, this is preferable to the local DC-side regulation of the dual-droop scheme.

B. Distributed control

We also consider the performance of the controller (13),(15) on the test networks under identical conditions, using the same droop coefficients $\tilde{Q} = \mathcal{K}$ for simplicity. In the simulation, we obtain $\bar{V}_k$ in (12) via propagation through the network with a communication delay of 10 ms between neighbouring buses. Simulations where $\bar{V}_k$ is evaluated via consensus schemes were also carried out and a similar performance was achieved for small communication delays < 10 ms, however the performance deteriorated significantly for larger communication delays. Figs. 8-9 show that the distributed controller regulates the voltages and frequencies of the hybrid AC/DC network to their nominal values while guaranteeing optimal power-sharing at steady-state.

V. CONCLUSION

We have proposed a new method for the control of inter-linking converter(s), used in conjunction with traditional droop control to guarantee stability and accurate power sharing in a general hybrid AC/DC network. The stability of the controlled system was proven and it was shown that power-sharing across the AC/DC network is significantly improved compared to dual-droop control. A secondary control scheme has also been
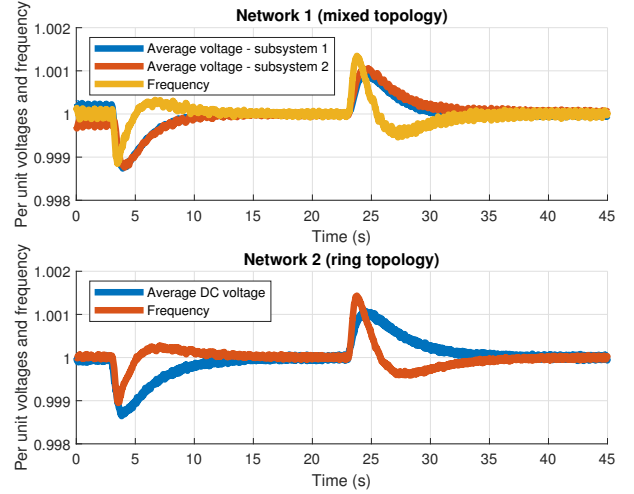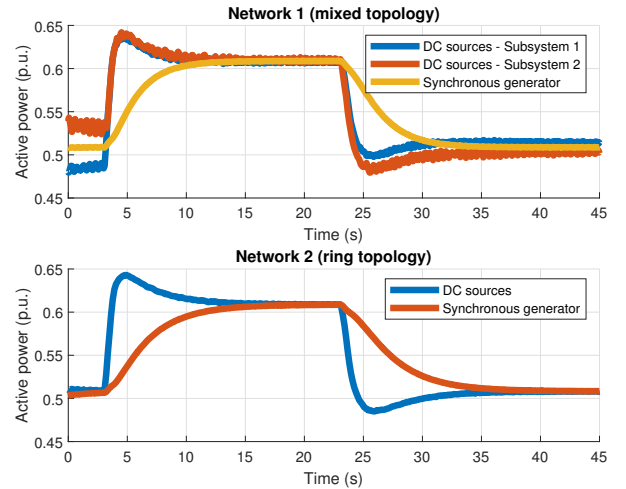

Figure 9. Power-sharing response with the distributed secondary controller (13),(15)

proposed that guarantees stability while achieving exact optimal power sharing and that bus frequencies and the weighted average of DC voltages return to their nominal values at steady state. Finally, the proposed algorithms were verified by simulation and compared to traditional dual-droop control.

APPENDIX

The appendix includes the proofs of the results presented in the main text. We provide first some notation that will be used within the proofs. Given some column vector z with length $|N|$, we use the subscripted vector z_{ac} to denote the vector that includes the elements of z with indices in N_{ac}, i.e. $z_{ac} = [z_{j,j \in N_{ac}}]$. Likewise the subscripts $z_{Gac}, z_{Xac}, z_{Xdc}, z_{dc}$ denote the vectors that include those entries for which $j \in N_{ac} \setminus X_{ac}$, $j \in X_{ac}$, $j \in X_{dc}$ and $j \in N_{dc}$ respectively. The following relations therefore hold: $z^T = [z_{ac}^T, z_{dc}^T]$, $z_{ac}^T = [z_{Gac}^T, z_{Xac}^T]$. For convenience we define $\Gamma > 0$ as the diagonal matrix of all $B_{ij}, (i,j) \in E_{ac}$, and G is defined as the conductance matrix of the DC subsystem(s); i.e. the Laplacian

weighted by the conductances G_{ij}. Finally, summation over all the DC subsystems is denoted by the shorthand $\sum_{k,dc}$.

Proof of Theorem 1: We prove our claim in Theorem 1 by finding a suitable Lyapunov function for the system (2), (6), (7b). Consider the following Lyapunov candidate:

$$W(\eta, \omega^G, V) = W_G + W_E + W_V$$
$$= \frac{1}{2}(\omega^G - \omega^{G*})^T M (\omega^G - \omega^{G*})$$
$$+ \mathbf{1}^T \Gamma \int_{\eta*}^{\eta} \sin(\phi) - \sin(\eta^*) d\phi + \frac{1}{2} m (V - V^*)^T C (V - V^*).$$
(16)

The time derivative of the first term is given by

$$\dot{W}_G = (\omega^G - \omega^{G*})^T (p_{Gac}^G - p_{Gac}^L - p_{Gac}^X + p_{Gac}^F - D\omega^G)$$
$$= (\omega^G - \omega^{G*})^T (p_{Gac}^G - p_{Gac}^L - p_{Gac}^X + p_{Gac}^F - D\omega^G)$$
$$+ (\omega^X - \omega^{X*})^T (p_{Xac}^G - p_{Xac}^L - p_{Xac}^X + p_{Xac}^F)$$

noting that the second expression follows by adding the term for the converter buses which is equal to zero by (1c). Using the equilibrium conditions (3), noting that p_{Gac}^X is a zero vector, and rearranging results to:

$$\dot{W}_G = (\omega - \omega^*)^T (p_{ac}^G - p_{ac}^{G*}) - (\omega^X - \omega^{X*})^T (p_{Xac}^X - p_{Xac}^{X*})$$
$$- (\omega - \omega^*)^T (p_{ac}^F - p_{ac}^{F*}) - (\omega^G - \omega^{G*})^T D(\omega^G - \omega^{G*}).$$
(17)

The time derivative of the second term in (16) is, again using the equilibrium conditions (3):

$$\dot{W}_E = (\Gamma(sin(\eta) - sin(\eta^*)))^T A^T (\omega - \omega^*)$$
$$= (\omega - \omega^*)^T (p_{ac}^F - p_{ac}^{F*}),$$

thus canceling the power transfer term in (17). The time derivative of W_V is given by:

$$\dot{W}_V = m(V - V^*)^T (p_{dc}^G - p_{dc}^{G*}) - m(V - V^*)^T (p_{dc}^X - p_{dc}^{X*})$$
$$- m(V - V^*)^T G(V - V^*). \quad (18)$$

Since G is the conductance matrix of the DC graph by definition we have $-m(V - V^*)^T G(V - V^*) \leq 0$ since $m > 0$. Furthermore, using (7b) and noting that $p_{X_x^{dc}}^X = -p_{X_x^{ac}}^X$:

$$m(V - V^*)^T (p_{dc}^X - p_{dc}^{X*}) = (\omega^X - \omega^{X*})^T (p_{Xdc}^X - p_{Xdc}^{X*})$$
$$= -(\omega^X - \omega^{X*})^T (p_{Xac}^X - p_{Xac}^{X*})$$

Hence the ILC terms in (17), (18) can be canceled out. We also note that converter buses X_{ac} have no frequency-dependent generation nor any damping, and that the respective entries of the diagonal matrix $\tilde{Q}$ are zeros, while all other entries of $\tilde{Q}$ are positive. Therefore, we define $\tilde{Q}_G > 0$ as the diagonal matrix with dimension $|N| - |X|$ which includes only the non-zero terms in $\tilde{Q}$. Putting it all together and substituting (6):

$$\dot{W} \leq - \begin{bmatrix} (\omega^G - \omega^{G*}) \\ m(V - V^*) \end{bmatrix}^T \tilde{Q}_G \begin{bmatrix} (\omega^G - \omega^{G*}) \\ m(V - V^*) \end{bmatrix}$$
$$- (\omega^G - \omega^{G*})^T D(\omega^G - \omega^{G*}) \leq 0. \quad (19)$$

Using Assumption 2, W_E has a strict local minimum at $\eta = \eta^*$. Likewise W_G and W_V have strict global minima at ω^{G*} and V^* respectively. Thus W has a strict minimum at $Z^* = (\eta^*, \omega^{G*}, V^*)$. Since ω^X is uniquely determined by V, we can then choose a neighbourhood of Z^* in the coordinates (η, ω^G, V). (19) further shows that W is a non-increasing function of time. Hence the connected set $T = \{(\eta, \omega^G, V) : W \leq \epsilon\}$ for some sufficiently small $\epsilon > 0$ is compact, forward-invariant and contains Z^*. We then apply LaSalle's Theorem, with W as the Lyapunov-like function, which states that all trajectories of the system starting from within T converge to the largest invariant set within T that satisfies $\dot{W} = 0$. Since both $\tilde{Q}_G$ and D are positive definite matrices, clearly $\dot{W} = 0$ implies $(\omega^G, V) = (\omega^{G*}, V^*)$ and therefore $\dot{\omega}^G = \dot{V} = 0$. This in turn implies by (3) that the converter AC-side frequencies $\omega^X = \omega^{X*}$. Furthermore, from the equilibrium conditions we deduce that the frequency in each AC subsystem synchronizes to a common value, hence the angle differences η converge also to some constant value. Therefore, by LaSalle's Theorem we have convergence to the set of equilibrium points as defined by (3). Finally, choosing S such that it is open, includes Z^*, and $S \subset T$ completes the proof. □

Proof of Theorem 2: From the equilibrium conditions (3), $[\omega^T \ mV^T]^T$ is arbitrarily close to the vector of equilibrium frequencies $\mathbf{1}\omega^*$ as the line resistances become arbitrarily small. This follows from the equilibrium conditions (3) and (1e), where if the conductances G_{ij} are arbitrarily large, the voltage differences $V_i - V_j$ are arbitrarily small. Therefore, to find the power allocation when the line resistances are arbitrarily small, we solve the equilibrium conditions:

$$-\tilde{Q}\mathbf{1}\omega^* + p_{nom}^G - p^L - p^X + p^F - p^u = 0$$
$$-\mathbf{1}^T \tilde{Q}\mathbf{1}\omega^* + \mathbf{1}^T p_{nom}^G - \mathbf{1}^T(p^L + p^u) - \mathbf{1}^T p^X + \mathbf{1}^T p^F = 0$$

Clearly $\mathbf{1}^T p^F = 0$ in a lossless network and $\mathbf{1}^T p^X = 0$ for lossless converters. Note also that the nominal power generation may be expressed as $p_{nom}^G = -\tilde{Q}\mathbf{1}\zeta$, where ζ is a constant. Hence, solving for $\mathbf{1}\omega^*$ and substituting into (6):

$$\mathbf{1}\omega^* = -\frac{\mathbf{1}\mathbf{1}^T}{\mathbf{1}^T \tilde{Q}\mathbf{1}}(p^L + p^u) - \mathbf{1}\zeta$$
$$p^G = -\tilde{Q}\mathbf{1}\omega^* - \tilde{Q}\mathbf{1}\zeta = \frac{\tilde{Q}\mathbf{1}\mathbf{1}^T}{\mathbf{1}^T \tilde{Q}\mathbf{1}}(p^L + p^u)$$

yields the solution (5) to the optimization problem (4). □

Proof of Theorem 3: This is analogous to that of Theorem 2. By premultiplying (15a) by $\mathbf{1}^T$ and noting (13) and the synchronization of frequencies at steady state, it follows that at equilibrium $\hat{\omega} = 0$. The latter shows from (15a) at steady state that $\xi^* = \mathbf{1}\bar{\xi}$ where $\bar{\xi}$ is the identical equilibrium value of the individual values ξ_j at node j. Then from the equilibrium conditions (3) we have:

$$\tilde{Q}\xi^* - p^L - p^X + p^F = 0 \quad (20a)$$
$$\mathbf{1}^T \tilde{Q}\xi^* - \mathbf{1}^T p^L - \mathbf{1}^T p^X + \mathbf{1}^T p^F = 0 \quad (20b)$$

Clearly $\mathbf{1}^T p^F = 0$ in a lossless network and $\mathbf{1}^T p^X = 0$ for lossless converters. Hence:

$$\mathbf{1}^T \tilde{Q} \mathbf{1} \bar{\xi} - \mathbf{1}^T p^L = 0 \tag{21a}$$

$$\xi^* = \mathbf{1}\bar{\xi} = \frac{\mathbf{1}\mathbf{1}^T p^L}{\mathbf{1}^T \tilde{Q} \mathbf{1}} \tag{21b}$$

Finally, substituting $p^G = \tilde{Q}\xi^*$ from (15b) into (21b) yields the solution to the optimization problem (4). $\square$

Proof of Theorem 4: We use $L = (1, 2, ...|L|)$ to represent the set of nodes of the communication graph. For convenience we also write the decomposition of $\tilde{Q}$ into its corresponding AC and DC terms as $\tilde{Q} = diag(\tilde{Q}_{ac}, \tilde{Q}_{dc})$ where $\tilde{Q}_{ac}$ and $\tilde{Q}_{dc}$ are diagonal matrices containing the inverse cost coefficients for the AC and DC generators respectively. Likewise, we decompose $\mathcal{K}$ into corresponding AC and DC matrices as $\mathcal{K} = diag(\mathcal{K}_{ac}, \mathcal{K}_{dc})$, where $\mathcal{K}_{ac} = \{\mathcal{K}_{jj} : j \in N_{ac}\}$ and $\mathcal{K}_{dc} = \{\mathcal{K}_{jj} : j \in N_{dc}\}$ are diagonal matrices of the corresponding gains in $\mathcal{K}$, appropriately ordered without loss of generality. We consider the following candidate Lyapunov function:

$$W = W_G + W_E + W_V + W_\xi \tag{22a}$$

$$= \frac{1}{2}(\omega^G)^T M \omega^G + \mathbf{1}^T \Gamma \int_{\eta^*}^{\eta} (sin(\phi) - sin(\eta^*)) d\phi$$

$$+ \frac{1}{2} m \bar{V}^T \bar{V} + \frac{1}{2}(\xi - \xi^*)^T T_\xi (\xi - \xi^*) \tag{22b}$$

The time derivatives of W_G are, again adding the term from (1c) and noting that $p_j^X = 0$ for all buses $j \in N_{ac} \setminus X_{ac}$:

$$\dot{W}_G = (\omega^G)^T (p_{Gac}^G - p_{Gac}^L + p_{Gac}^F - D\omega^G)$$

$$= (\omega^G)^T (p_{Gac}^G - p_{Gac}^L + p_{Gac}^F - D\omega^G)$$

$$+ (\omega^X)^T (p_{Xac}^G - p_{Xac}^L - p_{Xac}^X + p_{Xac}^F)$$

$$= (\omega)^T \tilde{Q}_{ac}(\xi_{ac} - \xi_{ac}^*) - (\omega^X)^T (p_{Xac}^X - p_{Xac}^{X*})$$

$$+ \omega^T (p_{ac}^F - p_{ac}^{F*}) - (\omega^G)^T (D + \mathcal{K}_{ac})\omega^G$$

The time derivatives of the other functions comprising W are:

$$\dot{W}_E = -(\Gamma(sin(\eta) - sin(\eta^*)))^T A^T \omega = -\omega^T (p_{ac}^F - p_{ac}^{F*})$$

$$\dot{W}_V = m\bar{V}^T \dot{V}$$

$$= m \sum_{k,dc} \bar{V}_k \sum_{j \in N_k^{dc}} [(p_j^G - p_j^{G*}) - (p_j^X - p_j^{X*})]$$

$$= m \sum_{k,dc} \bar{V}_k \sum_{j \in N_k^{dc}} (\tilde{Q}_{jj}(\xi_j - \xi_j^*) - \mathcal{K}_{jj}\bar{V}_k)$$

$$- m\bar{V}^T (p_{Xdc}^X - p_{Xdc}^{X*})$$

$$\dot{W}_\xi = (\xi - \xi^*)^T (-\mathcal{L}(\xi - \xi^*) - \tilde{Q}(\hat{\omega}))$$

$$= -(\xi - \xi^*)^T \mathcal{L}(\xi - \xi^*) - (\xi - \xi^*)^T \tilde{Q}\hat{\omega}$$

$$= -(\xi - \xi^*)^T \mathcal{L}(\xi - \xi^*) - \omega^T \tilde{Q}_{ac}(\xi_{ac} - \xi_{ac}^*)$$

$$- m \sum_{k,dc} \bar{V}_k \sum_{j \in N_k^{dc}} \tilde{Q}_{jj}(\xi_j - \xi_j^*)$$

using (10) and (11) to simplify $\dot{W}_V$. Clearly $-(\xi - \xi^*)^T \mathcal{L}(\xi - \xi^*) \leq 0$ from the definition of the Laplacian matrix $\mathcal{L}$. We also simplify further by cancelling like terms and thus obtain:

$$\dot{W} \leq -(\omega^G)^T (D + \mathcal{K}_{ac})\omega^G - (\omega^X)^T (p_{Xac}^X - p_{Xac}^{X*})$$

$$- m \sum_{k,dc} (\bar{V}_k \sum_{j \in N_k^{dc}} \mathcal{K}_{jj}\bar{V}_k) - m\bar{V}^T (p_{Xdc}^X - p_{Xdc}^{X*})$$

Noting that $-m \sum_{k,dc} (\bar{V}_k \sum_{j \in N_k^{dc}} \mathcal{K}_{jj}\bar{V}_k) \leq 0$ since $\mathcal{K}_{jj} \geq 0$ for all $j \in N$ and using (13) and $p_{X_x^{dc}}^X = -p_{X_x^{ac}}^X$ to cancel the second and fourth terms, we finally have:

$$\dot{W} \leq -(\omega^G)^T (D + \mathcal{K}_{ac})\omega^G \leq 0 \tag{23}$$

where the damping matrix D is positive definite and can be increased by proportional control of the AC sources via $\mathcal{K}_{ac}$. We then apply LaSalle's Theorem. Clearly, W is minimized at $\eta = \eta^*$, $\omega^G = 0$, $\bar{V} = 0$ and $\xi = \xi^*$. Therefore we consider the set T which includes $(\eta^*, 0, 0, \xi^*)$ and is defined by $\{(\eta, \omega^G, \bar{V}, \xi) : W \leq \epsilon\}$ for some positive constant ϵ. Since W is non-increasing with time, T is a compact, positively invariant set for ϵ sufficiently small. LaSalle's Theorem states that trajectories beginning in T converge to the largest invariant set within T for which $\dot{W} = 0$. We therefore examine the equality condition of (23). $\dot{W} = 0$ implies that $\omega^G = 0$, which from the system dynamics (2) implies that $\omega^X = m\bar{V} = 0$, $\bar{V} = 0$, and η is constant. Finally, from (15) if $\hat{\omega} = 0$ then $\mathcal{L}\xi = 0$ which from the definition of the Laplacian communication graph implies that all values $\xi_j, j \in L$ converge to some network-wide constant value $\bar{\bar{\xi}}$ and thus $\xi^* = \mathbf{1}\bar{\bar{\xi}}$. Hence the largest invariant set Ξ within T for which $\dot{W} = 0$ satisfies $(\eta, \omega^G, \bar{V}, \xi) = (\bar{\eta}, 0, 0, \bar{\bar{\xi}})$ for constant $\bar{\eta}$ and $\bar{\bar{\xi}}$. Furthermore, p^X trivially converges from (1c). To show that within Ξ, V takes some constant value $\hat{V}$ consider (1d) and (1e) and note that variables p^G, p^L and p^X are constant. Then defining $\underline{V}_j = V_j - \hat{V}_j$, it follows that the dynamics of $\underline{V}$ within Ξ satisfy $C\dot{\underline{V}} = -\mathcal{L}_{DC}\underline{V}$ where $\mathcal{L}_{DC}$ is the Laplacian of the graph (N_{dc}, E_{dc}), defined in analogy to (14). It is easy to see that the only invariant set of this linear ODE is $\underline{V} \in \text{Im}(\mathbf{1})$, where $\text{Im}(\mathbf{1})$ denotes the image of $\mathbf{1}$, which together with $\bar{V} = 0$ results to $\underline{V} = 0$. Therefore by LaSalle's theorem the trajectories of the system starting within T converge to the set of equilibrium points. This, in conjunction with Theorem 3 which suggests that equilibria of (1),(2),(12),(13),(15) are solutions to (4) completes the proof. $\square$

REFERENCES

[1] J. Watson and I. Lestas, "Frequency and voltage control of hybrid AC/DC networks," in *57th IEEE Conference on Decision and Control*, Dec. 2018.

[2] D. Jovcic *et al*, "Feasibility of DC Transmission Networks," *2011 IEEE Conference on Innovative Smart Grid Technologies Europe (ISGT Europe)*, 5-7 Dec. 2011.

[3] P. Wang *et al*, "Hybrid AC/DC Micro-Grids: Solution for High Efficiency Future Power Systems," in N.R. Karki et al. (eds.), *Sustainable Power Systems*, Reliable and Sustainable Electric Power and Energy Systems Management, Springer, 2017.

[4] S.M. Malik *et al*, "Voltage and frequency control strategies of hybrid AC/DC microgrid: a review," *IET Generation, Transmission and Distribution,* vol. 11, no. 2, 2017, pp. 303-313.

[5] E. Unamuno, J.A. Barrena, "Hybrid ac/dc microgrids - Part II: Review and classification of control strategies," *Renewable and Sustainable Energy Reviews*, vol. 52, December 2015, pp. 1123-1134.

[6] M. Cucuzzella, *et al*, "A Robust Consensus Algorithm for Current Sharing and Voltage Regulation in DC Microgrids," in *IEEE Transactions on Control Systems Technology*, vol. 27, No. 4, July 2019, pp. 1583-1595.

[7] T. Morstyn, B. Hredzak, G. D. Demetriades and V. G. Agelidis, "Unified Distributed Control for DC Microgrid Operating Modes," in *IEEE Transactions on Power Systems*, vol. 31, no. 1, Jan. 2016, pp. 802-812,.

[8] V. Nasirian, S. Moayedi, A. Davoudi and F. L. Lewis, "Distributed Cooperative Control of DC Microgrids," in *IEEE Transactions on Power Electronics*, vol. 30, no. 4, April 2015, pp. 2288-2303.

[9] L. Papangelis *et al*, "Coordinated Supervisory Control of Multi-Terminal HVDC Grids: a Model Predictive Control Approach," *IEEE Transactions on Power Delivery,* vol. 32, no. 6, Nov. 2017, pp. 4673-4683.

[10] J. Rocabert, *et al*, "Control of Power Converters in AC Microgrids," in *IEEE Transactions on Power Electronics*, vol. 27, no. 11, Nov. 2012, pp. 4734-4749.

[11] N. Chaudhuri, R. Majumder, and B. Chaudhuri, "System frequency support through multi-terminal DC (MTDC) grids," *IEEE Transactions on Power Systems*, vol. 28, Feb 2013, pp. 347–356.

[12] S. Akkari, J. Dai, M. Petit and X. Guillaud, "Interaction between the voltage-droop and the frequency-droop control for multi-terminal HVDC systems," in *IET Generation, Transmission & Distribution*, vol. 10, no. 6, 2016, pp. 1345-1352.

[13] S. M. Malik *et al*, "A Generalized Droop Strategy for Interlinking Converter in a Standalone Hybrid Microgrid," *Applied Energy,* vol. 226, 2018, pp. 1056-1063.

[14] H. Yoo, T. Nguyen and H. Kim, "Consensus-based Distributed Coordination Control of Hybrid AC/DC Microgrids," in *IEEE Transactions on Sustainable Energy*, in press, 2019.

[15] L. Papangelis *et al*, "A receding horizon approach to incorporate frequency support into the AC/DC converters of a multi-terminal DC grid," *Electric Power Systems Research,* vol. 148, 2017, pp. 1-9.

[16] P. C. Loh *et al*, "Autonomous Control of Interlinking Converter With Energy Storage in Hybrid AC–DC Microgrid," in *IEEE Transactions on Industry Applications*, vol. 49, no. 3, May-June 2013, pp. 1374-1382.

[17] F. Luo *et al*, "A Hybrid AC/DC Microgrid Control Scheme With Voltage-Source Inverter-Controlled Interlinking Converters", *Power Electronics and Applications (EPE'16 ECCE Europe), 18th European Conference on*, 2016.

[18] J. Dai and G. Damm, "An improved control law using HVDC systems for frequency control," in *Power Syst. Comput. Conf.*, 2011.

[19] M. Andreasson *et al*, "Distributed Frequency Control Through MTDC Transmission Systems," *IEEE Transactions on Power Systems,* vol. 32, no. 1, Jan. 2017, pp. 250-260.

[20] A. Ordoño, *et al*, "Interlinking converters and their contribution to primary regulation: a review," *International Journal of Electrical Power and Energy Systems*, vol. 111, 2019, pp. 44-57.

[21] T. Jouini *et al*, "Grid-Friendly Matching of Synchronous Machines by Tapping into the DC Storage," *IFAC-PapersOnLine*, vol. 49, issue 22, 2016, pp. 192-197.

[22] P. Monshizadeh, *et al*, "Stability and Frequency Regulation of Inverters with Capacitive Inertia," in *IEEE 56th Annual Conference on Decision and Control (CDC)*, 2017.

[23] F. Dörfler, M. Chertkov, and F. Bullo, "Synchronization in complex oscillator networks and smart grids", in *Proceedings of the National Academy of Sciences of the United States of America*, 2013.

[24] A. Kasis, E. Devane, C. Spanias, and I. Lestas, "Primary frequency regulation with load-side participation - Part I: stability and optimality," *IEEE Trans. Power Systems*, vol. 32, no. 5, Sept. 2017, pp. 3505-3518.

[25] M. Andreasson *et al*, "Distributed Controllers for Multi-Terminal HVDC Transmission Systems," *IEEE Transactions on Control of Network Systems,* vol. 4, no. 3, Sept. 2017, pp. 564-574.

[26] F. Thams, R. Eriksson and M. Molinas, "Interaction of Droop Control Structures and Its Inherent Effect on the Power Transfer Limits in Multiterminal VSC-HVDC," in *IEEE Transactions on Power Delivery*, vol. 32, no. 1, pp. 182-192, Feb. 2017.

[27] T.M. Haileselassie and K. Uhlen, "Impact of DC Line Voltage Drops on Power Flow of MTDC Using Droop Control," *IEEE Transactions on Power Systems,* vol. 27, no. 2, August 2012, pp. 1441-1449.

[28] F. Gao *et al*, "Primary and secondary control in DC microgrids: a review", *Journal of Modern Power Systems and Clean Energy*, vol. 7, 2019, pp. 227–242.